Magnetically recoverable Fe$_x$O$_y$–MWNT Fenton's catalysts that show enhanced activity at neutral pH

Meherzad F. Variava*, Tamara L. Church, Andrew T. Harris

Laboratory for Sustainable Technology, School of Chemical and Biomolecular Engineering, Building J01, The University of Sydney, NSW 2006, Australia

ARTICLE INFO

ABSTRACT

Known supported catalysts for the Fenton degradation of organic contaminants must be used in acidified solutions, where they leach Fe and consequently lose activity. In this study, Fe$_x$O$_y$ nanoparticles (average diameter = 3 nm) were immobilized onto multiwalled carbon nanotubes using a facile microwave-assisted polyol method to produce a Fenton catalyst that was active at neutral pH. Despite an Fe content of only 1.5 wt%, Fe$_x$O$_y$–MWNTs catalyzed the near-complete degradation of 50 mg L^{-1} of an organic dye contaminant in water at pH$_0$ = 7 in 30 min. At neutral pH, Fe leaching from the catalyst was minimal. Factors affecting the activity and stability of the catalyst were studied and a method was developed to regenerate the catalyst, which could be separated and reused with a small loss in activity.

1. Introduction

Fenton's reaction is the most common advanced oxidation process. These remove organic and inorganic contaminants from chemical wastewaters by oxidation, typically using the highly oxidizing ($E° = 2.8$ V) hydroxyl radical (HO$^\bullet$) as the oxidant [1–7]. In Fenton's reaction, HO$^\bullet$ radicals are formed from the decomposition of H$_2$O$_2$ over a lower-valent metal ion that can undergo a single-electron oxidation (Equation 1; M is a metal, typically Fe or Mn). In addition to the HO$^\bullet$ radical, the reaction produces a hydroxide ion (HO$^-$) and a higher-valent metal ion; the latter can oxidize H$_2$O$_2$ to regenerate the lower-valent metal ion (Eq. (2)). The combination of Eqs. (1) and (2) is the basis of Fenton's reaction [2,8,9]. For convenience, the metal ion is often introduced to the system as the higher-valent oxide (i.e. Fe^{3+}); this is sometimes referred to as a Fenton-like system.

$$H_2O_2 + M^{2+} \rightarrow M^{3+} + OH^- + HO^\bullet \tag{1}$$

$$H_2O_2 + M^{3+} \rightarrow M^{2+} + H^+ + HOO^\bullet \tag{2}$$
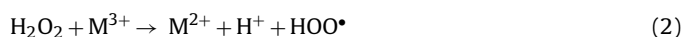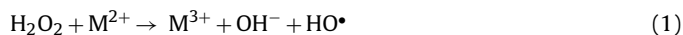
Fenton systems are typically homogenous and highly acidic, i.e., Fe^{3+} (*aq*) at pH = 2–4 [6,10,11], and thus have two major disadvantages: (i) ferric hydroxide sludge, formed due to the highly acidic reaction conditions, must be removed from the post-reaction

effluent and (ii) the highly acidic effluent must be neutralized prior to release to the environment [6,10,11]. Consequently, research is being undertaken on heterogeneous Fenton catalysts, typically supported on metal oxides, that can catalyze Fenton-like reactions at moderate pH values (4–10) [12–16] and can be re-used [6]. Composites based on Fe$_x$O$_y$ compounds are sensitive to acidic reaction conditions because Fe-containing particles are leached away from their supports [17,18]. Thus, although supported iron oxides are catalytically active and easily recoverable, their stability and ability to function at neutral pH remain topics of intensive research.

A supported iron oxide Fenton catalyst that is active at neutral pH would circumvent both the problems of catalyst leaching and the production of highly acidic effluent, and we considered the possibility that an iron oxide/carbon nanotube (CNT) catalyst may be active under these conditions. Carbon nanotubes (CNTs) are resistant to both acidic and basic media, and stable at temperatures up to 700 °C. Their mesoporosity and high surface area cause less mass-transfer resistance than traditional heterogeneous catalyst supports (e.g. activated carbon, alumina, zirconia and silica) [19–24]. High loadings of iron oxides (Fe$_2$O$_3$ and Fe$_3$O$_4$) on CNTs have proven active in Fenton degradation at pH ≤ 4 [14,25,26]. Most recently, Hu et al. [25] developed an Fe$_3$O$_4$-supported/multiwalled-carbon-nanotubes (MWNTs) composite (99 wt% Fe$_3$O$_4$) that catalyzed the oxidative degradation of 17α-methyltestosterone by H$_2$O$_2$. However, the high Fe$_3$O$_4$ loading (2 g L^{-1}) and low pH (pH$_0$ = 3.5) used in that system combined to cause Fe leaching that accounted for 30–40% of the observed degradation. To produce a catalyst that was active and stable

* Corresponding author. Tel.: +61 2 9351 2926; fax: +61 2 9351 2854.
  E-mail address: meherzad.variava@sydney.edu.au (M.F. Variava).

under neutral or near-neutral conditions, we modified a known polyol process [27–29] to develop a facile and rapid microwave-assisted method of functionalizing MWNTs with discrete iron oxide nanoparticles. We then tested the resulting Fe_xO_y–MWNT composites as catalysts for the oxidative degradation of a model azo dye, Orange G (OG), at neutral and near-neutral pH values. The effects of acidity and of H_2O_2 and catalyst concentration on the efficiency of the catalyst system were studied, as were catalyst reuse and Fe leaching.

2. Experimental

2.1. Chemicals

Poly(ethylene glycol) (190–200 g mol^{-1}, 97 wt%, Merck), ethanol (Absolute AR, Fronine), $FeCl_2 \cdot 4H_2O$ (>99 wt%, Sigma), H_2O_2 (*aq*, 30 wt%, Sigma–Aldrich), Orange G (OG, also called Acid Orange 10, $C_{16}H_{10}N_2Na_2O_7S_2$, 452 g mol^{-1}, >60 wt%, Sigma–Aldrich) and NaOH (98 wt%, Proanalys) were used as received.

2.2. Synthesis of MWNT composites

MWNTs were produced by chemical vapor deposition in a fluidized bed [30,31] and purified using a microwave technique previously described [32]. In a typical purification, as-synthesized MWNTs (200 mg) were added to H_2SO_4 (*aq*) (20 mL, 5 M) in a sealed, PTFE-lined, microwave-transparent pressure vessel. The vessel was transferred to a multimode microwave (MDS-10, Sineo Microwave Technology), heated at 20 °C min^{-1} to 220 °C and held at that temperature for 20 min, with the maximum power output of the magnetron limited to 1000 W. The purified products were then filtered through an ethanol-wetted, 0.5-μm PTFE membrane (Millipore), washed with deionized (DI) water, and dried in an oven at 110 °C.

The Fe_xO_y–MWNT composites were prepared by a polyol-mediated reaction under multimode microwave heating (MDS-10, Sineo Microwave Technology). Typically, purified MWNTs (100 mg) were sonicated in poly(ethylene glycol) (PEG, 5 g) for 30 min at high power to obtain a homogeneous mixture. $FeCl_2 \cdot 4H_2O$ (10 mg) was added and the mixture was stirred for 30 min. Separately, NaOH pellets (50 mg) were added to DI water (2 mL) and sonicated until dissolved. The resulting solution was added to the $FeCl_2 \cdot 4H_2O$/MWNT mixture, which was then stirred for a further 30 min at 30 °C. The resulting mixture was then sealed in a PTFE-lined, microwave-transparent pressure vessel, heated at 20 °C min^{-1} to 200 °C, and held at that temperature for 20 min, with the maximum power output of the magnetron limited to 600 W. The reaction mixture was cooled and ethanol was added and vigorously stirred to disperse the Fe_xO_y–MWNT composites homogeneously. These were then filtered through an ethanol-wetted, 0.5-μm hydrophilic PTFE membrane (Millipore) and washed with copious amounts of DI water to remove any residual PEG and unbound nanoparticles.

2.3. Catalyst characterization

For thermogravimetric analysis (TA SDT Q600), the sample (~10 mg) was heated at 5 °C min^{-1} to 1000 °C under instrument air (50 mL min^{-1}). For transmission electron microscopy (TEM), Fe_xO_y–MWNTs (~10 mg) were added to ethanol (15 mL) and the mixture was sonicated using a tip sonicator at high power for 10 min. Several droplets of the Fe_xO_y–MWNT/ethanol mixture were dropped onto a holey carbon film, supported on a 200 mesh copper grid, and dried in air. TEM studies were carried out on a Philips CM120 Biofilter operating at an accelerating voltage of 120 kV. The specific surface area (Brunauer–Emmett–Teller, S_{BET})

[33], pore size (Barrett–Joyner–Halenda, BJH, adsorption branch) [34], and pore volume of the composites were calculated from N_2 adsorption–desorption isotherms acquired at −196 °C on a Quantachrome Autosorb-1 apparatus. Samples were degassed at 180 °C and 0.005 mmHg for 6 h prior to analysis. X-ray photoelectron spectroscopy (XPS) was carried out using an ESCALAB250Xi (Thermo Scientific, UK) X-ray photoelectron spectrometer with monochromatized Al Kα X-rays as the excitation source. Additionally, narrow-scan photoelectron spectra (at 20 eV) were recorded for Fe 2p and C 1s. Raman spectra were recorded with a Raman spectrometer (InVia, Renishaw) using an Ar$^+$ ion laser at λ = 514.5 nm.

2.4. Catalytic oxidation of Orange G

The catalytic oxidation of Orange G (OG) was carried out in a 200-mL glass batch reactor under vigorous stirring at 35 °C. In a typical test, the dye (5 mg) was dissolved in DI water (90 mL) and the solution was allowed to stabilize at the desired temperature. For some experiments, the pH of this solution was adjusted by adding NaOH (*aq*, 1 M) or H_2SO_4 (*aq*, 1 M), or an $HPO_4^{2-}/H_2PO_4^-$ buffer. An appropriate amount of H_2O_2 (*aq*) was diluted in DI water (5 mL) and this solution was added to the stirred dye solution. Separately, the Fe_xO_y–MWNT (50 mg, 1.5 wt% Fe) catalyst was dispersed in DI water (5 mL) under low-intensity ultrasound for 20 min before the mixture was added to the dye solution. Thus the concentration of dye at the outset of the catalytic degradation reaction was 50 mg L^{-1}. Aliquots were removed and filtered through a syringe filter before analysis by UV–vis spectroscopy (Cary 50 UV–vis spectrophotometer) and the dye degradation was monitored by the change in absorbance at λ = 480 nm. At high absorbance the absolute error of the UV–vis spectrometer was 0.001 Abs with a relative error of 0.1%. At low absorbance the absolute error was 0.002 Abs, with a relative error of 4%. However, the final values of the absorbance were compared to a calibrated graph of known dilutions to check for drift (or lack of) in the instrument. The final [H_2O_2] was determined semi-quantitatively using peroxide test strips (Quantofix, MACHEREY-NAGEL).

Fourier transform infrared (FT-IR) spectroscopy was carried out using a Nicolet 6700 (Thermo Scientific, UK) spectrometer with an attenuated total reflectance (ATR) accessory employing a diamond crystal.

3. Results and discussion

3.1. Synthesis and characterization of Fe_xO_y–MWNT composites

The MWNTs used as catalyst supports were produced by chemical vapor deposition in a fluidized bed, and purified in the microwave to yield >97 wt% MWNTs (Supplementary Content, Figs. S1 and S2). A polyol-mediated solvothermal reaction [35,36] was used to deposit iron oxides onto the purified MWNTs. Polyols (organic compounds possessing at least two hydroxyl groups) can act as both reducing and chelating agents, and can therefore be used to produce discrete nanosized particles from aqueous metal ions [35,37]. In the case of iron, an $FeCl_2 \cdot 4H_2O$ precursor is hydrolyzed to $Fe(OH)_2$, which is subsequently converted to a mixed Fe(II)/Fe(III) oxide, identified as Fe_3O_4, at elevated temperature (>200 °C) [38]. To date, the polyol-based functionalization of MWNTs with Fe_3O_4 has been performed using $FeCl_3 \cdot 6H_2O$ as a precursor and in a traditionally heated autoclave, and therefore required reaction times of 1.5–12 h [27–29]. Microwave irradiation can increase the rate of a reaction through rapid, homogeneous heating [39–42], and has been applied to the polyol functionalization of Pt and various Pt–metal combinations [35,36]. We therefore used microwave heating in the polyol-assisted deposition of Fe_xO_y onto MWNTs, and produced Fe_xO_y–MWNTs in only 30 min. The final Fe loading
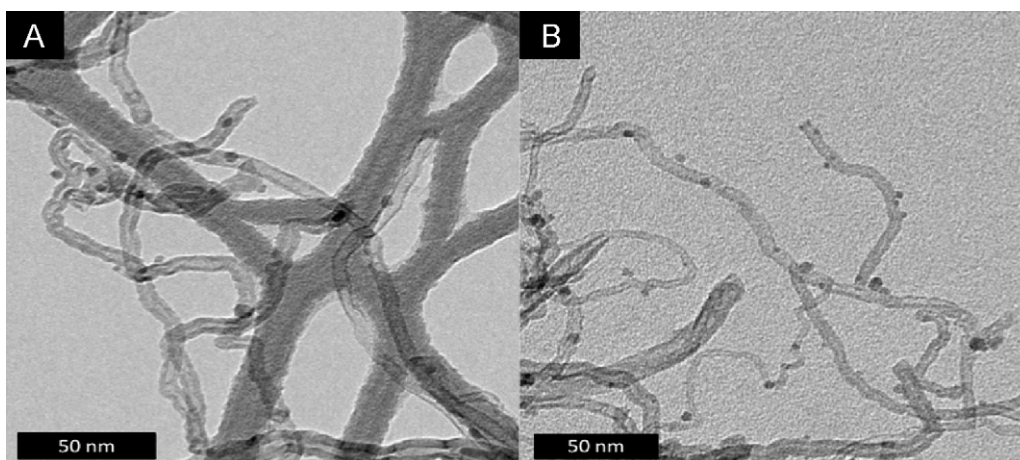
Fig. 1. (A) and (B) Transmission electron micrographs (TEM) of Fe_xO_y–MWNTs (1.5 wt% Fe). Average particle size $d_{avg} = 3.0 \pm 0.8$ nm.

on the Fe_xO_y–MWNTs was 1.5 wt%. Despite the short reaction time used, TEM images of the functionalized MWNTs showed a uniform, homogeneous and non-agglomerated coverage of Fe_xO_y on the MWNT surface. The average size of the supported Fe_xO_y nanoparticles, calculated by measuring 500 randomly chosen particles in the TEM images (Fig. 1), was 3.0 ± 0.8 nm. The relatively small supported Fe_xO_y particles obtained were likely the result of the heating rate used ($20\,^\circ$C min^{-1}). Elevated heating rates accelerate the reduction and nucleation of metal nanoparticles, facilitating the formation of smaller particles rather than larger agglomerates [35], and a similar effect has been proposed for metal–oxide particles [27]. However, we did not investigate the effects of the Fe source or glycol used on particle size.

Although the Fe_xO_y–MWNT composites were vigorously sonicated during TEM sample preparation, no free nanoparticles were observed, attesting to the strong attachment of the metal–oxide particles to the MWNTs. These observations are consistent with the functionalization mechanism proposed by Wang et al. [27], in which very fine, high-energy Fe_3O_4 subparticles are formed and deposited on MWNTs. Further Fe_3O_4 particles are attracted to these subparticles by van der Waals forces and magnetic interactions [43]. The glycol stabilizes the particles at a critical size, preventing further agglomeration and resulting in well-dispersed Fe_xO_y nanoparticles on the MWNTs.

N_2 adsorption–desorption isotherms of the purified and Fe_xO_y-functionalized MWNTs were IUPAC Type II (Fig. S3), indicating that both materials were mesoporous. The powdered Fe_xO_y-functionalized MWNT composite had a larger average interparticle pore diameter (39.9 nm) and smaller pore volume (1.84 mL g^{-1}) than the purified MWNTs (Table 1).

The chemical nature of the composites was investigated using Raman spectroscopy, X-ray photoelectron spectroscopy (XPS), and X-ray diffraction (XRD). Both the purified MWNTs and the Fe_xO_y–MWNT composites (Fig. 2) showed the two intense Raman
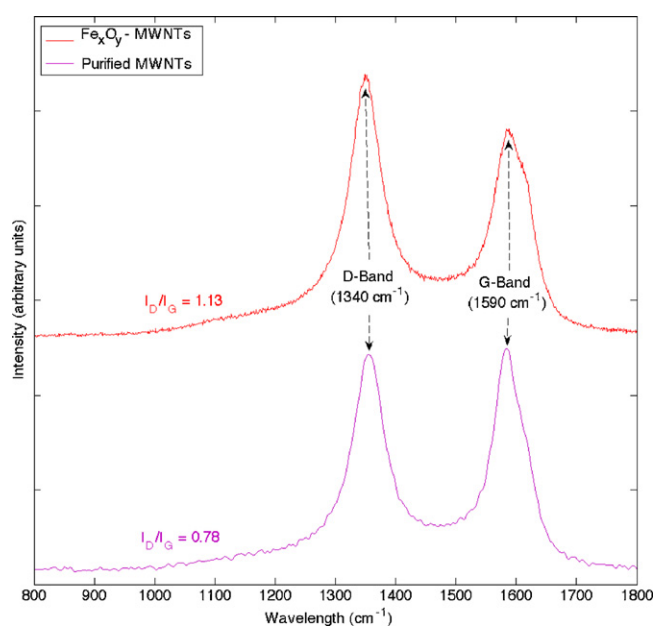

Fig. 2. Raman spectra of purified and Fe_xO_y-functionalized MWNTs.

peaks that are typical of CNT samples: the D band at 1340 cm^{-1}, attributed to defects and disorder in the walls of the MWNTs, and the G band at 1590 cm^{-1}, attributed to the C—C stretching mode of ordered graphitic carbon [44–46]. The intensity ratio of the peaks, I_D/I_G, indicates the degree of disorder in the walls of the graphitic tubes within MWNT systems. I_D/I_G was 0.78 for the purified MWNTs, indicating good crystallinity, as expected given the synthesis and purification methods used [32]. However, the Fe_xO_y–MWNT composites had $I_D/I_G = 1.13$, implying that the

Table 1
Surface and porosity properties of the purified and Fe_xO_y-functionalized MWNTs.[a]

	S_{BET} [m^2 g^{-1}]	d_{pore} [nm]	V_{pore} [cm^3 g^{-1}]
MWNTs	246	16.2	2.02
Fe_xO_y–MWNTs	210	39.9	1.84
Fe_xO_y–MWNTs, used[b]	160	10.0	0.46
Fe_xO_y–MWNTs, used and regenerated[c]	200	31.0	1.05

[a] Determined from N_2 adsorption–desorption isotherms recorded at $-196\,^\circ$C; see Fig. S3. S_{BET} = BET surface area, measured over P/P_0 = 0.05–0.35; d_{pore} = average pore size, calculated via BJH theory from the adsorption branch; V_{pore} = total pore volume, calculated via BJH theory for P/P_0 = 0.995.

[b] Fe_xO_y–MWNTs were used in the 1-h degradation of 0.11 mM OG.

[c] Fe_xO_y–MWNTs were used in the 1-h degradation of 0.11 mM OG, and then regenerated using 1-M NaOH (aq). See Section 2 for details.
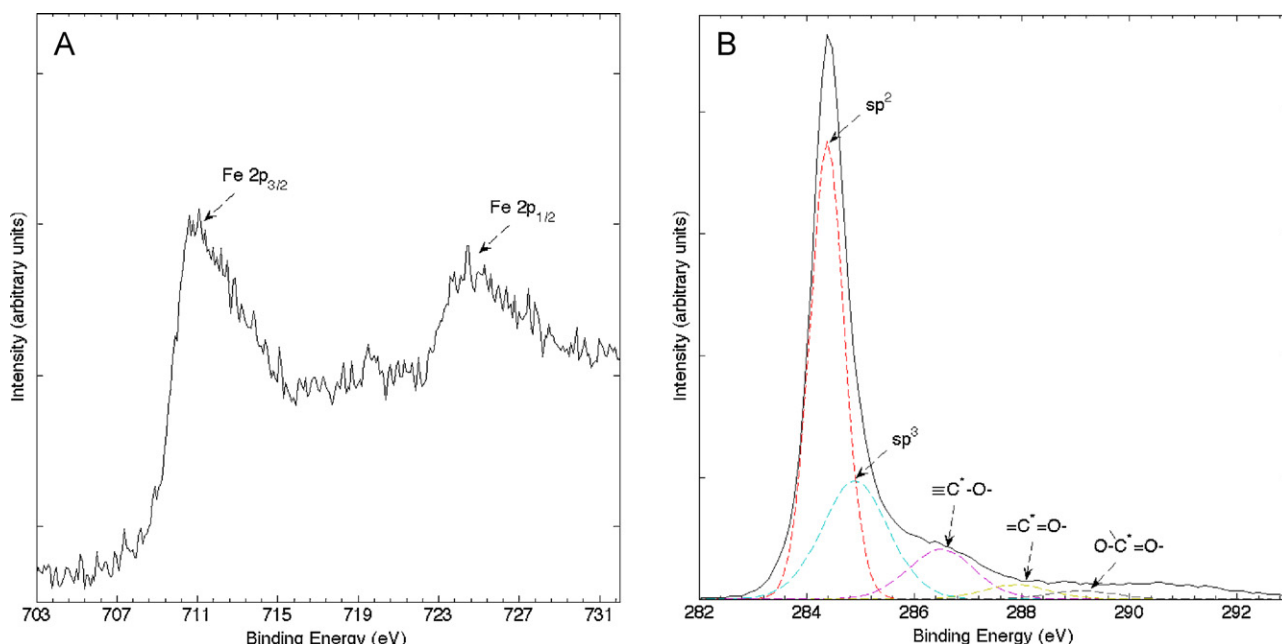
Fig. 3. X-ray photoelectron spectra of the Fe_xO_y–MWNT composites (1.5 wt% Fe). (A) Core-level scan of Fe 2p peaks. (B) Core-level scan of C 1s peaks.

functionalization process decreased the MWNT crystallinity. Consistent with the Raman spectroscopy results, the C1s core level XPS spectrum of Fe_xO_y–MWNT composites (Fig. 3b) confirmed the significant presence of C sp^2 bonds, whose binding energy (BE) of 284.5 eV was characteristic of graphitic carbon bonds in MWNTs [47–49]. Deconvolution of the C1s core level spectrum also indicated the presence of sp^3 C—C bonds (defects), as well as both sp^3 and sp^2 carbons bonded to oxygen ($\equiv C^*$—O, BE = 286.5 eV; >C^*=O, BE = 287.7 eV). The sp^3 carbons and C—O bonds were likely introduced during MWNT purification, which required concentrated acid (5 M H_2SO_4) and high temperatures (>200 °C).
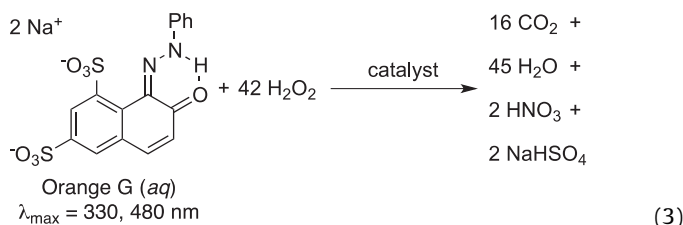
The surface oxidation states of the deposited Fe_xO_y particles were also studied by XPS. As most of the Fe atoms were in nanosized agglomerates, the measured oxidation state offers an appropriate representation of the Fe atoms throughout the system. Fe $2p_{3/2}$ and Fe $2p_{1/2}$ were detected at BE = 711 eV and 724.7 eV, respectively, in an intensity ratio of Fe $2p_{3/2}$/Fe $2p_{1/2}$ = 1.02 (Fig. 3a), similar to reported values for Fe_3O_4 [50,51] and for γ-Fe_2O_3 [52,53]. The small differences between the BE values (<0.1 eV between the measured values and those reported for Fe_3O_4) are within the range of variation that can be caused by surface charge compensation [50,54]. The result was further investigated by XRD. In order to obtain a sufficient signal-to-noise ratio, this analysis was carried out using a sample of Fe_xO_y–MWNT with slightly larger Fe content (3.5 wt%). This sample was synthesized by the same polyol method as the catalytic sample. The XRD pattern (Fig. S9) most closely matched that of cubic Fe_3O_4 ($FeFe_2O_4$; JCPDS 26-1136); however, we cannot discount the presence of inverse-spinel Fe_3O_4 or γ-Fe_2O_3 in our catalyst based upon the XRD pattern, as both of these compounds produce diffraction patterns similar to that of cubic Fe_3O_4.

3.2. Decomposition of Orange G using Fe_xO_y–MWNTs

3.2.1. Catalytic degradation

The activity of the Fe_xO_y–MWNT composites as Fenton's catalysts was studied using OG dye as a model reactant. OG exists preferentially as the hydrazone tautomer in polar solvents [55], and requires 42 equivalents of H_2O_2 for complete mineralization (Eq. (3)). In H_2O, OG exhibits an absorption band at 480 nm,

and its degradation can therefore be monitored by the change in absorbance at that wavelength, as per Eq. (4).

$$2\ Na^+ \quad \text{Orange G (aq)} \quad + 42\ H_2O_2 \xrightarrow{\text{catalyst}} \begin{array}{l} 16\ CO_2\ + \\ 45\ H_2O\ + \\ 2\ HNO_3\ + \\ 2\ NaHSO_4 \end{array}$$

Orange G (*aq*)
λ_{max} = 330, 480 nm

(3)

$$\frac{Abs_t}{Abs_0} = a[OG]_t + b \tag{4}$$

where a and b are constants related to $[OG]_0$

The degradation of OG dye in aqueous solution was investigated under a range of experimental conditions. Control experiments revealed that neither H_2O_2 nor the Fe_xO_y–MWNT composites, applied individually, degraded the dye significantly (Fig. S4). This is consistent with previous work [55,56], and reasonable based upon the low oxidation potentials of H_2O_2 and Fe_3O_4 (1.78 V and 0.77 V, respectively; cf. 2.80 V for HO•). OG, an anionic dye, will adsorb on positively charged surfaces, meaning that it will adsorb onto surfaces at pH values lower than their respective points of zero charge (PZCs); the pH_{PZC} values of Fe_3O_4 and γ-Fe_2O_3 are 7 [57] and 6.6 [5,58], respectively, and that of MWNTs is 4.9 [59,60]. Under the catalysis conditions (pH_0 = 7), but in the absence of H_2O_2, OG adsorption onto the Fe_xO_y–MWNT catalyst was ~6%; whereas on unfunctionalized MWNTs it was only 2%, consistent with the higher PZC of Fe_3O_4 and γ-Fe_2O_3 than MWNTs. Thus rapid and selective adsorption of OG occurs at the catalytic Fe-based sites at pH = 7. A small amount of OG degradation was observed when only MWNTs and H_2O_2 were added to the reaction mixture (Fig. S4). This has also been observed for the Fenton degradation of a related dye, Orange II, catalyzed by carbon supports [14], and the Fenton degradation of phenol catalyzed by MWNTs [26]. Thus, the MWNTs themselves may be weakly active Fenton catalysts, though we cannot rule out contributions from impurities derived from the Fe/Al_2O_3 catalyst used to produce the MWNTs.
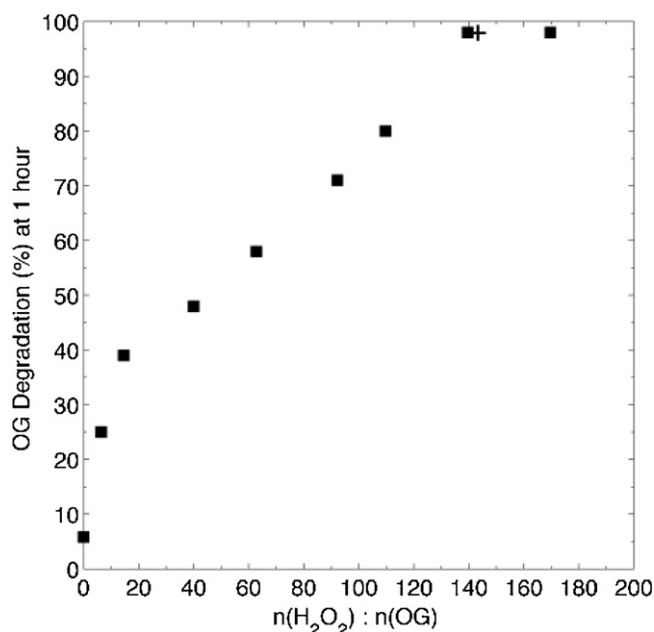
Fig. 4. Effect of H_2O_2 dosage on OG degradation after 1 h. $[OG]_0 = 0.11$ mM, $T = 35\,°C$, 50 mg of Fe_xO_y–MWNT catalyst, $pH_0 = 7$, total volume = 100 mL. (+) $[OG] = 0.22$ mM.

When both H_2O_2 and Fe_xO_y–MWNTs were present, significant dye degradation occurred (Fig. S5). The rate of dye degradation was unchanged when the reaction was performed in the dark (Table S1), demonstrating that a photo-assisted mechanism, which has been observed for the Fe_2O_3/C-catalyzed degradation of a related dye [61], was not significant in the present system. The degradation of OG could not accurately be modeled using simple kinetics, as is also the case for its homogeneous Fenton degradation [16], so a precise rate law could not be written. Nevertheless, the effects of various parameters on the reaction were investigated.

3.2.2. Effect of H_2O_2 and Fe_xO_y–MWNT concentrations

We began by examining the effect of H_2O_2 concentration on OG degradation catalyzed by Fe_xO_y–MWNTs. The performance of a Fenton system depends on a critical H_2O_2 concentration. More $HO^•$ is produced by Eq. (1) at higher H_2O_2 concentrations; however, when H_2O_2 concentration is too high, degradation is slowed because $HO^•$ radicals are scavenged according to Eqs. (5)–(7) [9,14,62]. $HOO^•$ radicals, formed by the reaction of H_2O_2 with Fe^{3+} (Equation 2) or $HO^•$ (Eq. (5)) have an oxidation potential of 1.70 V, and can also degrade organics, though much more slowly. For example, the second-order rate constant for the reaction of Orange II, a dye whose structure is similar to that of OG, with $HO^•$ is $\sim 10^3 \times$ faster than that with $HOO^•$ [61].

$$H_2O_2 + HO^• \rightarrow H_2O + HOO^• \qquad (5)$$

$$HOO^• + HO^• \rightarrow H_2O + O_2 \qquad (6)$$

$$2HO^• \rightarrow H_2O_2 \qquad (7)$$

In our system, when $n(H_2O_2):n(OG)$ was below 110, the reaction essentially stopped before all of the OG had been consumed (Figs. 4 and S5). This was true even when there was enough H_2O_2 to completely mineralize OG (Eq. (3)), so the H_2O_2 was not simply consumed by the decomposition products of OG. Better OG removal was achieved using excess H_2O_2, and the final absorbance at 480 nm decreased to only 4% of its initial value as $n(H_2O_2):n(OG)$ increased to 140 (Fig. 4). At the end of the reaction $[H_2O_2]$ was in the range 0.059–0.147 mM, down from 15.4 mM. Thus, more H_2O_2 than required for OG degradation was consumed, possibly due to
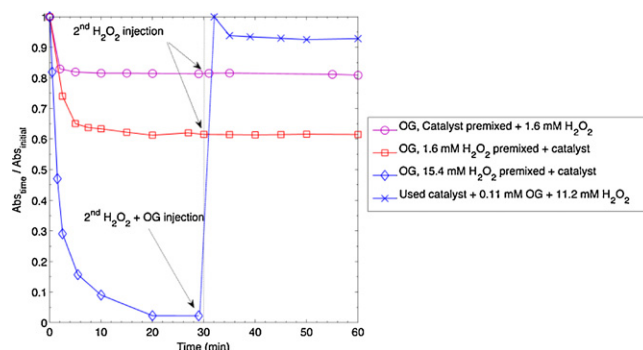

Fig. 5. Effect of multiple H_2O_2 injections on OG degradation. $[OG]_0 = 0.11$ mM, $T = 35\,°C$, 50 mg of Fe_xO_y–MWNT catalyst, $pH_0 = 7$, total volume = 100 mL.

disproportionation owed to the large excess of H_2O_2. The excess is a trade-off with traditional Fenton systems, which require less H_2O_2 but must be carried out in acidified environments [1,5,14]. However, the loss of H_2O_2 via side reactions cannot fully account for the incomplete OG degradation, as a second injection of H_2O_2 did not induce further degradation (Fig. 5). Moreover, no further gains in final conversion were obtained when $n(H_2O_2):n(OG)$ was raised to 170. The degradation performance of Fe_xO_y–MWNTs at $n(H_2O_2):n(OG) = 140$ was maintained when the concentrations of both OG and H_2O_2 were doubled ($[OG]_0 = 0.22$ mM; see Fig. 4) to produce a 100-mg L^{-1} OG solution, which is an applicable industrially emitted effluent concentration [63]. Thus Fe_xO_y–MWNT degrades OG at industrially relevant concentrations without the 'high' concentration of H_2O_2 (31 mM) considerably slowing the reaction, despite that the scavenging of $HO^•$ radicals by H_2O_2 has been witnessed for $[H_2O_2] > \sim 5$ mM [14,64].

The amount of OG that was degraded before the reaction stopped also depended on the amount of catalyst present (Fig. 6). Thus, although 0.5 g L^{-1} of Fe_xO_y–MWNTs could degrade 96% of the OG in a 0.11-mM solution (i.e. $n(Fe_xO_y)/n(\text{substrate}) = 0.41$) when $[H_2O_2]_0 = 15.4$ mM, only 18% of the dye was degraded when 0.05 g L^{-1} Fe_xO_y–MWNTs was used. Therefore, the catalyst concentration could not be significantly lowered without a loss in
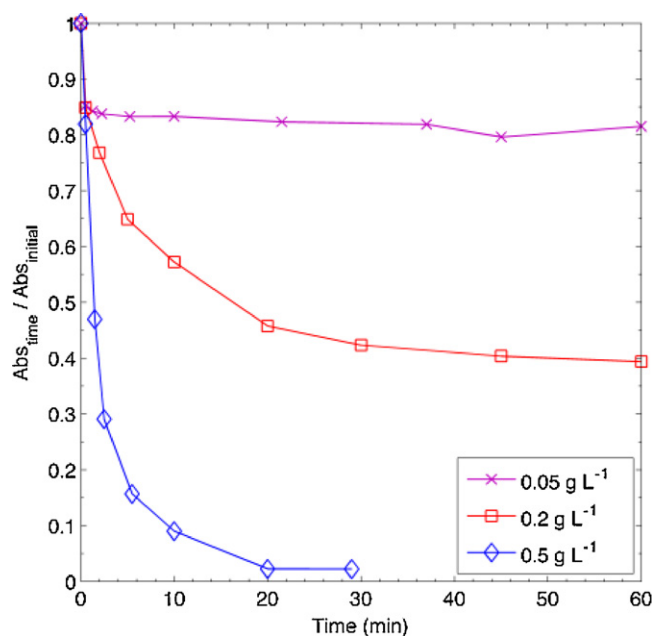

Fig. 6. Effect of catalyst loading on OG degradation. $[OG]_0 = 0.11$ mM, $n(H_2O_2):n(OG) = 140$, $T = 35\,°C$, $pH_0 = 7$, total volume = 100 mL.

degradation ability. Nevertheless, the Fe_xO_y–MWNT catalyst produced here was active at much lower catalyst loading than a related MWNT–Fe_3O_4 catalyst used at $n(Fe_3O_4)/n(substrate) > 10^5$ [25]. This may be attributed to the polyol process used to produce the present catalyst, as it gave small Fe_xO_y nanoparticles and therefore more catalytic surface area.

Given that Fe_xO_y–MWNTs could not always completely degrade OG dye even when sufficient H_2O_2 was available or when multiple H_2O_2 injections were used, and that less degradation was achieved when less H_2O_2 or catalyst were used, we suspected that the catalyst was deactivated over time. The large difference in reaction rates for Eqs. (1) and (2) caused us to consider the possibility that the reaction slowed to a near-halt whenever all of the Fe^{2+} ions that were initially present had produced a single equivalent of $HO^•$ and were thereby converted to Fe^{3+} ions; however, this hypothesis was rejected based on the results obtained for $[Fe_xO_y$–MWNT$] = 0.5\,g\,L^{-1}$, when $n(Fe_3O_4)/n(OG) = 0.41$ (Figs. S4 and S6). The OG absorbance could be completely removed under these conditions, demonstrating that Fe^{2+} was regenerated on the timescale of the reaction. Moreover, the XPS spectrum of the spent catalyst (Fig. S6a) was very similar to that of the fresh catalyst, and the XRD pattern (Fig. S9) of a Fe_xO_y–MWNT catalyst with 3.5 wt% Fe was also unchanged after being used to degrade OG under the highest H_2O_2 excess used here ($n(H_2O_2):n(OG) = 140$). Catalyst deactivation may instead have been caused by the complexation of Fe sites by OG or its oxidation products [9] at pH < 7; this could inhibit their catalytic activity. For example, Fe^{3+} cannot oxidize H_2O_2 (Eq. (2)) to form $HOO^•$ and Fe^{2+}, which in turn forms the active $HO^•$ radicals, unless the Fe^{3+} ion bears at least one open coordination site or labile ligand [65]. This hypothesis was supported by the observation that less OG could be degraded under a particular set of reaction conditions when the catalyst and dye were mixed 20 min before H_2O_2 was added (Fig. 5). However, H_2O_2 is clearly reduced by the Fe_xO_y–MWNT catalysts early in the reaction, as rapid OG degradation does occur, and OG can be completely degraded if the catalyst loading and initial excess of H_2O_2 are sufficient. Thus, inhibition by adsorption became more significant over the course of the reaction, likely for two reasons. The dye-degradation products, which, consistent with literature reports [54,63], included carboxylic acids (visible in an infrared spectrum of the product mixture, see Fig. S7), may have bound to the Fe ions more strongly than the dye itself did. Additionally, the formation of such degradation products, and possibly of CO_2 from mineralization, acidified the reaction mixture. After 30 min, the reaction pH fell from 7 to 6.2 for $n(H_2O_2):n(OG) = 40$, when little OG degradation was observed, and to as low as 4.8 for $n(H_2O_2):n(OG) = 110$. As a result, the surface of the Fe-containing particles became more positively charged, causing negatively charged dyes or other electron-donor ligands to adsorb more strongly. Even upon basification of the inactive solution (initial $n(H_2O_2):n(OG) = 40$, 30 min) to pH = 8, no further degradation was possible, even with further addition of H_2O_2. This suggests that the oxygen-containing decomposition products, rather than OG, were likely bound to Fe.

3.2.3. Effect of pH

To better understand the influence of pH in this system, OG degradations were carried out at initial pH values (pH_0) of 4–10 (Fig. 7; $n(H_2O_2):n(OG) = 90$). The most complete degradation, 82%, was observed for $pH_0 = 8$. Slightly less degradation occurred in neutral or slightly acidic solutions ($pH_0 = 6$ or 7). The rate of H_2O_2 degradation over Fe ions is higher at elevated pH [66,67], and this may have favored the reaction at $pH_0 = 8$. Moreover, more OG adsorbed on the catalyst at lower pH values (Fig. S8), and this may have inhibited its activity.
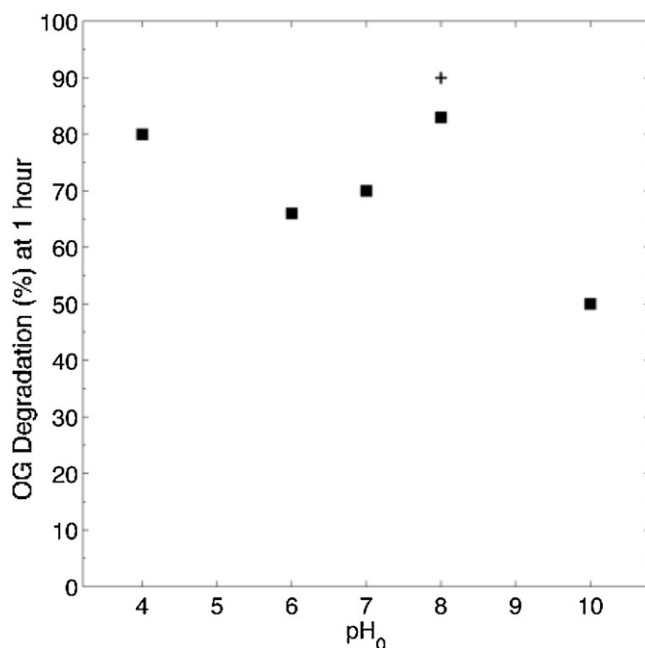

Fig. 7. Effect of initial solution pH, pH_0, on OG degradation after 1 h. $[OG]_0 = 0.11\,mM$, $T = 35\,°C$, 50 mg of Fe_xO_y–MWNT catalyst, $n(OG):n(H_2O_2) = 90$, total volume = 100 mL. (+) pH was maintained with a $HPO_4^{2-}/H_2PO_4^-$ buffer.

At $pH_0 = 4$, below the PZC of MWNTs, adsorption on the catalyst removed ∼12% of the OG absorbance, nearly three times the value observed for $pH_0 = 8$ (see Fig. S8). Nevertheless, OG degradation was only slightly slower at $pH_0 = 4$ than at $pH_0 = 8$, and was faster than at $pH_0 = 6$ or 7. Performing the reaction at low pH_0 is undesirable for practical reasons, so we did not thoroughly investigate the high activity at $pH_0 = 4$; however, a significant amount of Fe was solubilized under these conditions. An XPS spectrum of the catalyst used at $pH_0 = 4$ showed a final Fe loading of 1.2 wt%, meaning that 20% of the initial Fe had been leached into solution. The resulting dissolved Fe ions could have accounted for the greater reaction rate at $pH_0 = 4$ (leaching was minimal at $pH_0 = 7$; see Section 3.2.4). When the reaction was performed at a constant pH of 8 ($HPO_4^{2-}/H_2PO_4^-$ buffer), >90% of the OG was degraded, demonstrating the beneficial effect of minimizing the adsorption of organics onto the active sites. Although HPO_4^{2-} and $H_2PO_4^-$ can scavenge $HO^•$, the reaction is expected to occur ∼$10^2 \times$ slower than the reaction between $HO^•$ and OG. The second-order rate constants for the reactions of $HO^•$ with HPO_4^{2-} (>90% of buffer) and Orange II (an OG-like dye) are on the order of 10^5 [68] and 10^9 [69], respectively. Thus the tenfold excess of HPO_4^{2-} is not expected to be a significant scavenger. When pH_0 was increased to 10 in order to further decrease adsorption, OG degradation suffered even though H_2O_2 was consumed (final $[H_2O_2] < 0.059\,mM$; cf. $[H_2O_2]_0 = 1.0\,mM$). This is attributed to the disproportionation of H_2O_2 into O_2 and H_2O, which is faster in alkaline solutions [70], and which would decrease the availability of H_2O_2.

3.2.4. Catalyst reuse

The commercial applicability of the novel Fe_xO_y–MWNT catalyst will depend critically on its potential for reuse; its deactivation by adsorption is thus problematic. Moreover, after catalyzing the decomposition of OG ($n(OG):n(H_2O_2) = 140$, $pH_0 = 7$), the spent Fe_xO_y–MWNT catalyst had $S_{BET} = 160\,m^2\,g^{-1}$, a 30% decrease from the value before use, and the average pore size and pore volume dropped to 10 nm and 0.462 $cm^3\,g^{-1}$, respectively (Table 1). Thus,

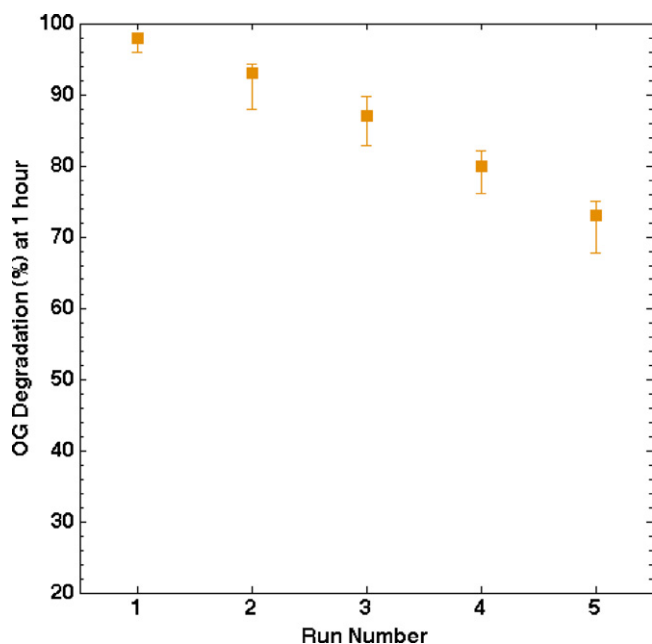**Fig. 8.** Effect of repeated catalyst use on OG degradation. $[OG]_0 = 0.11$ mM, $T = 35\,°C$, $t = 1$ h, 50 mg of Fe_xO_y–MWNT catalyst, $n(OG):n(H_2O_2) = 140$, $pH_0 = 7$, total volume = 100 mL.

although adsorption clearly played a significant role in deactivating the catalyst active sites, the mesoporous nature of the catalytic supports was also impacted. Zazo et al. also observed large decreases in the surface area and pore volume of Fe_2O_3-activated carbon following its use as a Fenton catalyst, and attributed these effects to the formation of polymeric byproducts [56]. They were able to partially restore the activity of their catalysts by washing with 1-M NaOH (*aq*), and we therefore attempted to separate and regenerate the Fe_xO_y–MWNTs. Isolation was performed using magnetic separation, a method well-suited to recovering supported magnetite (and possibly maghemite) from solution. The Fe_xO_y–MWNTs were subjected to a strong magnetic field, and the residual solution was decanted. Even at the low Fe loading employed (1.5 wt% Fe), the Fe_xO_y–MWNTs were very responsive to an external magnetic field. The separated catalysts were washed with NaOH (1 M, 100 mL), magnetically separated again, further washed with DI water, and dried at 120 °C. The reactivated Fe_xO_y–MWNT catalysts showed only minor reductions in activity in subsequent OG degradations (Fig. 8). The regeneration treatment also markedly improved the surface properties of the Fe_xO_y–MWNTs, elevating the S_{BET}, pore size, and pore volume to 200 $m^2\,g^{-1}$, 31 nm, and 1.05 $cm^3\,g^{-1}$, respectively, after a single use and regeneration (Table 1). Thus, adsorbed reaction products may have contributed to the decrease in surface area and pore volume that occurred over the course of the reaction; this would allow the porous structure to be recovered when the compounds were washed away. Additionally, XPS analyses of the pristine catalyst and the catalyst thrice recovered and regenerated did not show a significant loss of iron; $\Delta[Fe]$ was 0.1% and TEM images of the spent catalyst revealed little change in the particle size (average particle diameter 3 ± 1 nm (Fig. S6b); cf. 3.0 ± 0.8 nm in the fresh catalyst). This is in contrast to the cases of Fe_2O_3 on activated carbon [56] and Fe_3O_4 on porous carbon [14], both used at $pH_0 = 3$; these lost significant amounts of Fe over the course of the reaction. Assuming that approximately equal amounts of Fe leached during each catalytic run in our system, <2 ppm Fe was lost per reaction; this is an accepted concentration of iron in treated streams [71].

4. Conclusion

Fe_xO_y-functionalized MWNTs were produced from $FeCl_2 \cdot 4H_2O$ and PEG-200 using a novel polyol-mediated microwave-assisted method. This method obviated tedious chemical preparations of the MWNT surface prior to the decoration with nanoparticles. The microwave-assisted reaction provided for rapid and consistent heating, producing a homogeneous system for the nucleation and growth of Fe nanoparticles. The Fe_xO_y–MWNT composites contained well-dispersed Fe nanoparticles with an average particle size of 3.0 ± 0.8 nm; the small particle size was critical to maximizing the active surface area of the Fe catalyst, and may have contributed significantly to the high catalytic activity of the Fe_xO_y–MWNT composites.

The Fe_xO_y–MWNT composites reduced H_2O_2, and thus catalyzed the Fenton-like degradation of OG, at a low catalyst concentration ($0.5\,g\,L^{-1}$) and without an acidified reaction mixture. Residual dye and OG-decomposition products adsorbed on the catalyst active sites and even the support; this was aggravated by the decrease of pH as the reaction proceeded, and eventually caused catalyst deactivation. However, basic treatment regenerated the spent catalysts, allowing them to be reused with very little loss of Fe. The catalytic activity, stability and reusability of these low-Fe-loaded heterogeneous catalysts in neutral aqueous solution ($pH_0 = 6$–8) is promising for their use in wastewater and effluent treatment because the resulting solution requires neither the neutralization of a highly acidic material, nor treatment to remove dissolved Fe ions. Future work on this system will endeavor to lower the amount of H_2O_2 required for a successful reaction. Also, the losses of catalytic activity after multiple runs, likely caused by iron leaching and active surface area, will need to be studied in some detail in order to shed more light on the industrial recyclability of the catalyst.

Appendix A. Supplementary data

Supplementary data associated with this article can be found, in the online version, at http://dx.doi.org/ 10.1016/j.apcatb.2012.04.034.

References

[1] A. Rodríguez, G. Ovejero, J.L. Sotelo, M. Mestanza, J. García, Industrial and Engineering Chemistry Research 49 (2010) 498–505.
[2] K.M. Parida, A.C. Pradhan, Industrial and Engineering Chemistry Research 49 (2010) 8310–8318.
[3] A. Santos, P. Yustos, S. Rodriguez, E. Simon, A. Romero, Industrial and Engineering Chemistry Research 49 (2010) 5583–5587.
[4] T. Rhadfi, J.-Y. Piquemal, L. Sicard, F. Herbst, E. Briot, M. Benedetti, A. Atlamsani, Applied Catalysis A 386 (2010) 132–139.
[5] T.L.P. Dantas, V.P. Mendonça, H.J. José, A.E. Rodrigues, R.F.P.M. Moreira, Chemical Engineering Journal 118 (2006) 77–82.

[6] E.G. Garrido-Ramírez, B.K.G. Theng, M.L. Mora, Applied Clay Science 47 (2010) 182–192.
[7] P.R. Gogate, A.B. Pandit, Advances in Environmental Research 8 (2004) 501–551.
[8] W.P. Kwan, B.M. Voelker, Environmental Science and Technology 37 (2003) 1150–1158.
[9] C. Walling, Accounts of Chemical Research 8 (1975) 125–131.
[10] S.-F. Kang, C.-H. Liao, M.-C. Chen, Chemosphere 46 (2002) 923–928.
[11] S. Perathoner, G. Centi, Topics in Catalysis 33 (2005) 207–224.
[12] M. Cheng, W. Song, W. Ma, C. Chen, J. Zhao, J. Lin, H. Zhu, Applied Catalysis B 77 (2008) 355–363.
[13] M. Cheng, W. Ma, J. Li, Y. Huang, J. Zhao, Y.X. Wen, Y. Xu, Environmental Science and Technology 38 (2004) 1569–1575.
[14] J.H. Ramirez, F.J. Maldonado-Hódar, A.F. Pérez-Cadenas, C. Moreno-Castilla, C.A. Costa, L.M. Madeira, Applied Catalysis B 75 (2007) 312–323.
[15] M.B. Kasiri, H. Aleboyeh, A. Aleboyeh, Applied Catalysis B 84 (2008) 9–15.
[16] S.-P. Sun, C.-J. Li, J.-H. Sun, S.-H. Shi, M.-H. Fan, Q. Zhou, Journal of Hazardous Materials 161 (2009) 1052–1057.
[17] Q. Wu, X. Hu, P.L. Yue, X.S. Zhao, G.Q. Lu, Applied Catalysis B 32 (2001) 151–156.
[18] E.V. Kuznetsova, E.N. Savinov, L.A. Vostrikova, V.N. Parmon, Applied Catalysis B 51 (2004) 165–170.
[19] M. Trépanier, A. Tavasoli, A.K. Dalai, N. Abatzoglou, Applied Catalysis A 353 (2009) 193–202.
[20] K.H. Chuang, Z.S. Liu, C.Y. Lu, M.Y. Wey, Industrial and Engineering Chemistry Research 48 (2009) 4202–4209.
[21] W. Deng, M. Liu, X. Tan, Q. Zhang, Y. Wang, Journal of Catalysis 271 (2010) 22–32.
[22] H. Kong, M. Zhou, G.-D. Lin, H.-B. Zhang, Catalysis Letters 135 (2010) 83–90.
[23] H.L. Pang, J.P. Lu, J.H. Chen, C.T. Huang, B. Liu, X.H. Zhang, Electrochimica Acta 54 (2009) 2610–2615.
[24] O. Winjobi, Z. Zhang, C. Liang, W. Li, Electrochimica Acta 55 (2010) 4217–4221.
[25] X. Hu, B. Liu, Y. Deng, H. Chen, S. Luo, C. Sun, P. Yang, S. Yang, Applied Catalysis B 107 (2011) 274–283.
[26] Q. Liao, J. Sun, L. Gao, Colloids and Surfaces A 345 (2009) 95–100.
[27] H.T. Wang, L.L. Cao, S.C. Yan, N.P. Huang, Z.D. Xiao, Materials Science and Engineering B 164 (2009) 191–194.
[28] Y. Zhan, R. Zhao, Y. Lei, F. Meng, J. Zhong, X. Liu, Applied Surface Science 257 (2011) 4524–4528.
[29] B. Jia, L. Gao, J. Sun, Carbon 45 (2007) 1476–1481.
[30] J. Liu, A.T. Harris, AIChE Journal 56 (2010) 102–113.
[31] C.H. See, K.J. MacKenzie, O.M. Dunens, A.T. Harris, Chemical Engineering Science 64 (2009) 3614–3621.
[32] J. Liu, O.M. Dunens, K.J. Mackenzie, C.H. See, A.T. Harris, AIChE Journal 54 (2008) 3303–3307.
[33] S. Brunauer, P.H. Emmett, E. Teller, Journal of the American Chemical Society 60 (1938) 309–319.
[34] E.P. Barrett, L.G. Joyner, P.P. Halenda, Journal of the American Chemical Society 73 (1951) 373–380.
[35] Z. Liu, J.Y. Lee, W. Chen, M. Han, L.M. Gan, Langmuir 20 (2004) 181–187.
[36] W. Zhang, J. Chen, G.F. Swiegers, Z.-F. Ma, G.G. Wallace, Nanoscale 2 (2010) 282–286.
[37] S. Laurent, D. Forge, M. Port, A. Roch, C. Robic, L. Vander Elst, R.N. Muller, Chemical Reviews 108 (2008) 2064–2110.
[38] D. Caruntu, Y. Remond, N.H. Chou, M.-J. Jun, G. Caruntu, J. He, G. Goloverda, C. O'Connor, V. Kolesnichenko, Inorganic Chemistry 41 (2002) 6137–6146.
[39] C.O. Kappe, Angewandte Chemie International Edition 43 (2004) 6250–6284.
[40] Z. Guo, Y. Chen, L. Li, X. Wang, G.L. Haller, Y. Yang, Journal of Catalysis 276 (2010) 314–326.
[41] C.-T. Hsieh, W.-M. Hung, W.-Y. Chen, J.-Y. Lin, International Journal of Hydrogen Energy 36 (2011) 2765–2772.
[42] Z. Gan, X. Zheng, D. Wei, Q. Hu, A. Zhao, X. Zhang, G. Li, Superlattices and Microstructures 47 (2010) 705–709.
[43] J. Wan, X. Cai, J. Feng, X. Meng, E. Liu, Journal of Materials Chemistry 17 (2007) 1188–1192.
[44] S. Osswald, M. Havel, Y. Gogotsi, Journal of Raman Specroscopy 38 (2007) 728–736.
[45] M.S. Dresselhaus, G. Dresselhaus, R. Saito, A. Jorio, Physics Reports 409 (2005) 47–99.
[46] S. Costa, E. Borowiak-Palen, Acta Physica Polonica A 116 (2009) 32–35.
[47] L. Stobinski, B. Lesiak, L. Kövér, J. Tóth, S. Biniak, G. Trykowski, J. Judek, Journal of Alloys and Compounds 501 (2010) 77–84.
[48] H. Ago, T. Kugler, F. Cacialli, W.R. Salaneck, M.S.P. Shaffer, A.H. Windle, R.H. Friend, Journal of Physical Chemistry B 103 (1999) 8116–8121.
[49] P. Hojati-Talemi, R. Cervini, G.P. Simon, Journal of Nanoparticle Research 12 (2010) 393–403.
[50] C.S. Kuivila, J.B. Butt, P.C. Stair, Applied Surface Science 32 (1988) 99–121.
[51] Y. Tian, B. Yu, X. Li, K. Li, Journal of Materials Chemistry 21 (2011) 2476–2481.
[52] X. Teng, D. Black, N.J. Watkins, Y. Gao, H. Yang, Nano Letters 3 (2003) 261–264.
[53] B.J. Tan, K.J. Klabunde, P.M.A. Sherwood, Chemistry of Materials 2 (1990) 186–191.
[54] B.L. Maschhoff, N.R. Armstrong, Langmuir 7 (1991) 693–703.
[55] A.A. MacKay, J.J. Pignatello, Helvetica Chimica Acta 84 (2001) 2589–2600.
[56] J.A. Zazo, J.A. Casas, A.F. Mohedano, J.J. Rodríguez, Applied. Catalysis B 65 (2006) 261–268.
[57] M. Abili Nejad, M. Jonsson, Journal of Nuclear Materials 345 (2005) 219–224.
[58] L. Garcell, M.P. Morales, M. Andres-Vergés, P. Tartaj, C.J. Serna, Journal of Colloid and Interface Science 205 (1998) 470–475.
[59] C. Lu, H. Chiu, Chemical Engineering Science 61 (2006) 1138–1145.
[60] C.-Y. Kuo, C.-H. Wu, J.-Y. Wu, Journal of Colloid and Interface Science 327 (2008) 308–315.
[61] T. Yuranova, O. Enea, E. Mielczarski, J. Mielczarski, P. Albers, J. Kiwi, Applied Catalysis B 49 (2004) 39–50.
[62] M.R. Rojas, F. Pérez, D. Whitley, R.G. Arnold, A.E. Sáez, Industrial and Engineering Chemistry Research 49 (2010) 11331–11343.
[63] D. Wambuguh, R.R. Chianelli, New Journal of Chemistry 32 (2008) 2189–2194.
[64] J. Feng, X. Hu, P.L. Yue, H.Y. Zhu, G.Q. Lu, Industrial and Engineering Chemistry Research 42 (2003) 2058–2066.
[65] E. Graf, J.R. Mahoney, R.G. Bryant, J.W. Eaton, Journal of Biological Chemistry 259 (1984) 3620–3624.
[66] S. Chou, C. Huang, Chemosphere 38 (1999) 2719–2731.
[67] S.-S. Lin, M.D. Gurol, Environmental Science and Technology 32 (1998) 1417–1423.
[68] P. Maruthamuthu, P. Neta, Journal of Physical Chemistry 82 (1978) 710–713.
[69] V. Nadtochenko, J. Kiwi, Faraday Transactions 93 (1997) 2373–2378.
[70] W.D. Nicoll, A.F. Smith, Industrial and Engineering Chemistry 47 (1955) 2548–2554.
[71] Agriculture and Resource Management Council of Australia and New Zealand; Guidelines for Sewerage Systems: Acceptance of Trade Waste (Industrial Waste), 1994.